*Journal of Aircraft and Spacecraft Technology*

Original Research Paper

# On Wing Tip Flow Around a Low Aspect Ratio Wing at Low Flight Speeds Using OpenFOAM® and Parallel Processing

**[1]Nikolaos Konstantinos Lampropoulos and [2]Ioannis Eleftherios Sarris**

*[1]Division of Aerodynamics and Flight Mechanics, Hellenic Air Force Academy, Dekelia Air Base, Acharnes Attikis, Tatoi, Greece*
*[2]Department of Mechanical Engineering, University of West Attica, 250 Thivon P. Ralli Str., Athens, Greece*

*Article history*
Received: 21-08-2024
Revised: 19-09-2024
Accepted: 26-09-2024

Corresponding Author:
Nikolaos Konstantinos Lampropoulos
Division of Aerodynamics and Flight Mechanics, Hellenic Air Force Academy, Dekelia Air Base, Acharnes Attikis, Tatoi, Greece
Email: nikolaoslampropoulos@hotmail.com

**Abstract:** In the present study, the effect of the wing tip geometry on the aerodynamic performance of a swept-back wing at moderate Reynolds numbers is investigated through numerical simulation and parallel processing. The aim is the identification of streamlines around the wing and subsequently the formation of the wing tip vortex. Due to the purely three-dimensional character of the flow, the turbulence is resolved with advanced modeling, i.e., the Improved Delayed Detached Eddy Simulation (IDDES) which is well customized to switch modes between Large Eddy Simulation (LES) and Reynolds Averaged Navier Stokes (RAS) thus increasing the accuracy in the shear layer regions, the tip vortex and the wake while at the same time keeping the computational cost at reasonable levels. The simulation of the flow verifies the positive effect of rounding the wing tip, in comparison to flat/cut-off configuration, in terms of increase of lift, reduction of downwash, and induced drag under cruise conditions. By maneuvering conditions the rounded tip wing fails to obstruct the formation of the wing tip vortex, nevertheless, it also delivers well in terms of aerodynamic performance.

**Keywords:** Improved Delayed Detached Eddy Simulation (IDDES), Wing-Tip Vortex

## Introduction

The wing tip vortex's inception and evolution are of paramount importance in aeronautical engineering. This is due not only to the hazards posed by the trailing vortices to the following aircraft but also to the aerodynamic performance degradation of the wings themselves. The latter phenomenon is more prominent by swept-back wings which tend to tip stall due to the induced span-wise flow of the boundary layer from root to tip, as reported by Soltani *et al*. (2017). Subsequently, the tip stalling causes the center of pressure of the wing to move forward, affecting the pitching moment of the aircraft, see Antoniou *et al*. (2023). The correct identification of the wig tip vortex is critical for swept back wing designs on the following grounds: Firstly, it induces the span-wise flow from the inboard part of the wing to the tip due to low pressure in the vortex region and secondly, it affects the up wash and downwash which in turn lead to the inclination of the lift vector and the production of additional drag. This induced drag reduces the endurance of the aircraft but also hinders the acceleration during take-off since it may contribute up to 80% of total drag for commercial airliners such as the A320 at low speeds and high angles of attack, Rajendran (2012). To this end, the evolution of the wing tip vortex is investigated both numerically and experimentally in the bibliography. Starting from the less computationally intensive methods, namely the linear eddy viscosity turbulence models (URANS), it was proven that although the mean flow was predicted reasonably well the turbulent structures near the tip were not accurately identified as stated by O'Regan *et al.* (2016). This was primarily due to the inadequacy of the Boussinesq Approximation for modeling the anisotropic nature of turbulence in the highly rotational vortex which leads to an over-prediction of the turbulence viscosity within the vortex core and in turn results in its increased decay rate, as reported by Feder *et al*. (2018). More advanced turbulence modeling, namely Detached Eddy Simulation (DES) was implemented by simulation of wing tip vortex in order to address the aforementioned deficiencies. Liang and Xue (2014) investigated with DES the flow around NACA0012 airfoil at high AoA and moderate Reynolds numbers showing that the RANS-Spalart-Allmaras (RANS-SA) model underpredicts the peak value of axial

vorticity in the vortex by 25-40% (depending on the AoA) whereas DES agrees quite well with the experiment. RANS-SA also underpredicted the minimum pressure in the core at several downstream locations, in comparison to DES, thus hinting that the model does not deliver well by wing-tip vortex flows. A more advanced method such as LES was used by Jiang *et al*. (2008) by the prediction of tip vortex shedding from a rectangular half-wing with a NACA 0012 airfoil section and a rounded wing tip at a high Reynolds number ($4.6\times10^6$). They verified that the rotation of the tip vortex produces low pressure in the core region which accelerates the axial flow and produces axial velocity whose instantaneous value can be as large as $2.0\times U_\infty$.

The objective of the present study is to enhance the aerodynamic performance of a wing by rounding the tip. The investigation is implemented by cross-comparison of the simulated flows around a cut-off and a rounded tip at several flight conditions. These comprise the level flight/cruise regime and the cruise speed/high AoA maneuvering conditions. The turbulence model is the IDDES as proposed by Philippe (1997). The Computational Fluid Dynamics (CFD) code used herein is OpenFOAM® and the meshing is enabled by means of the commercial mesh generator Pointwise™. The computational resources were provided by the national High-Performance Computing platform ARIS.

### *Numerical Procedure*

### *Turbulence Modeling*

The unsteady turbulent flow is simulated through the use of the IDDES model which has its origin in the RANS SA one equation turbulence model. The latter solves a transport equation for the viscosity-like variable *v(tilde)* which reads as follows:

$$\frac{\partial \tilde{\nu}}{\partial t} + u_j \frac{\partial \tilde{\nu}}{\partial x_j} + c_{b1}\hat{S}\tilde{\nu}(1-f_{t2}) - \left[c_{w1}f_w - \frac{c_{b1}}{\kappa^2}f_{t2}\right]\left(\frac{\tilde{\nu}}{d}\right)^2 + \frac{+1}{\sigma}\left[\frac{\partial}{\partial x_j}\left((\tilde{\nu}+\nu)\frac{\partial \tilde{\nu}}{\partial x_j}\right) + \sigma_{b2}\left(\frac{\partial \tilde{\nu}}{\partial x_j}\right)^2\right] \quad (1)$$

The turbulent eddy viscosity is given by: $\mu_t = \rho\, \nu(tilde)\, f_{v1}$. In the SA-DES model, the wall distance $d$ in Eq. (1) is replaced by the length scale $\tilde{d}$ that enters the turbulence model and controls the eddy viscosity: $\tilde{d} \equiv min(d, C_{DES}\Delta)$, where d is the wall distance, $C_{DES}$ is of order 1 and $\Delta \equiv max(\Delta_x, \Delta_y, \Delta_z)$ is the chosen measure of grid spacing as proposed by Spalart *et al*. (2006). This formulation enables the DES model to work in dual mode. The first one (RANS mode) is enabled near the wall where the computational mesh is very stretched, thus the turbulence can not be resolved but it is taken into account by the turbulent viscosity in accordance with Boussinesq assumption, and the second one (LES mode) is activated far from the wall. The latter region (outer zones of the boundary layer, shear layers, wake) can be resolved with meshes comprising near cubic-sized hexahedra having comparable size with the large eddies which carry about 70-80% of turbulence. In this way, the Navier-Stokes equations are solved in a purely unsteady manner for all turbulence scales that can be identified by the grid whereas the contribution of the smaller eddies to turbulence is estimated by the turbulence model which acts as a subgrid-scale model. Lately, Spalart *et al*. (2006) proposed an improvement to the standard DES model (Delayed DES or DDES) which preserves RANS mode, namely it prohibits the model from switching to LES mode, therefore attempting to resolve the turbulence in regions where the mesh isotropy and density is not adequate, thus leading to underestimation of turbulence levels. An advanced version of DES, the Improved DES (IDDES) as proposed by Shur *et al*. (2008) which has enhanced wall modeling is adopted in this study aiming at better identification of vortical structures and the formation, in general, of the wing tip vortex.

## Materials and Methods

The present work is exclusively computational. The softwares used herein are OpenFOAM® and Pointwise™. The computational resources are 10 nodes (20@2.8 GHz (two sockets) without accelerator (64 GB RAM)). All nodes are connected via Infiniband network and share 2PB GPFS storage. The node island is based on the IBM NeXtScale platform and on Intel Xeon E5-2680v2 processors.

### *Numerical Methods*

The CFD code being used in this study is the open source software package OpenFOAM® which is released under the GNU General Public License. The simulation is transient through a second-order implicit backward temporal discretization scheme which implements the time marching by using the current and the two previous updated values of variables in the calculation of the temporal derivative. The convective terms are discretized by a second-order scheme which is a mix of linear and upwind methods, thus being a good compromise between accuracy (linear) and numerical stability (upwinding). The Navier-Stokes equations are solved by the PIMPLE Algorithm which is a combination of PISO (Pressure Implicit with Splitting of Operator) and SIMPLE (Semi-Implicit Method for Pressure-Linked Equations). This algorithm retains the numerical stability of the code, even at Courant numbers higher than one, and thus is well formulated for DES simulations on meshes with dozens of millions of computational cells which can hardly be handled even by HPC platforms. The method aims the increase the time step up to a value that enables the adequate temporal discretization of the vortical structures in the shear layer, the tip vortex, and the wake

**DOI: 10.3844/jastsp.2025.1.11**

where the LES mode is activated. On the other hand in the regions of the flow where high aspect ratio cells are used (near the wall boundaries), the transient character of the simulation is compromised, due to the relatively high time step, but this comes at the moderate expense of accuracy since the turbulence, in these regions, is not resolved by the RANS mode but being simply estimated through the Boussinesq assumption. Therefore, we have a mixed algorithm that runs on unsteady mode in LES regions and steady state in RANS ones, thus saving considerably in computational resources.

### *Meshing and Code Set-Up*

The computational meshes being used for both cases, i.e., flat and rounded wing tips, are block-structured as depicted in Fig. (1). Both pressure and suction side of airfoils have 220 points while 30 points are placed in the trailing edge and 300 points in the spanwise direction. In both cases, the inflation layers are produced through a hyperbolic extrusion method which enables high orthogonality metrics. In terms of the flat tip, the mesh is restricted by a plane at the tip spanwise location. Thus, the mesh in the vortex and the wake region can be readily constructed through an extrusion in the spanwise direction. On the other hand, the block meshes around the rounded wing are formed by the projection of patches of the surface mesh on a dome surrounding the wing and subsequent stitching of the blocks. The FWT and RWT meshes have a scale of about 43 million cells while the first node is at distance $ds = 2\times10^{-5}\ m$ off the wall which meets the requirement $y^+ < 1$ for adequate resolution of the laminar sublayer. The size of the wing and the boundaries of the computational meshes are depicted in Fig. (2) (left). The dimension of the turbulence length scale in the vortical structures is estimated by Eq. (2) at a diameter $L_T = 0.02\ m$ through a prior RANS (k-ε) model simulation. This is the size of large eddies carrying most of the energy contents which are meant to be resolved by an adequately dense isotropic mesh. The cell size in highly turbulent regions is selected to be about 5 *mm* and the time step $dt = 1\times10^{-5}\ sec$ which is expected to be small enough for the accurate temporal resolution of vortices (LES regions) while it ensures the numerical stability of the RANS mode in the highly stretched mesh region near the wall boundary. Special attention is given to the wing tip and near wake region (up to one tip chord downstream), Fig. (2), middle, where nearly cubic cells are achieved. Thus the switch of the turbulence model to LES mode is enabled in order to capture the phenomenon of wake formation and the downwash, Fig. (2), right. Finally, grid independence is verified by an additional simulation on a coarser mesh for the FWT case. This mesh (FWT COARSE), being 15.5 million cells big, has the same density in the inflation layer region whereas it is considerably coarser in the wing tip vortex region (both spanwise and chordwise):

$$C_m^{\frac{3}{4}} \frac{k^{\frac{3}{4}}}{L_T} \tag{2}$$

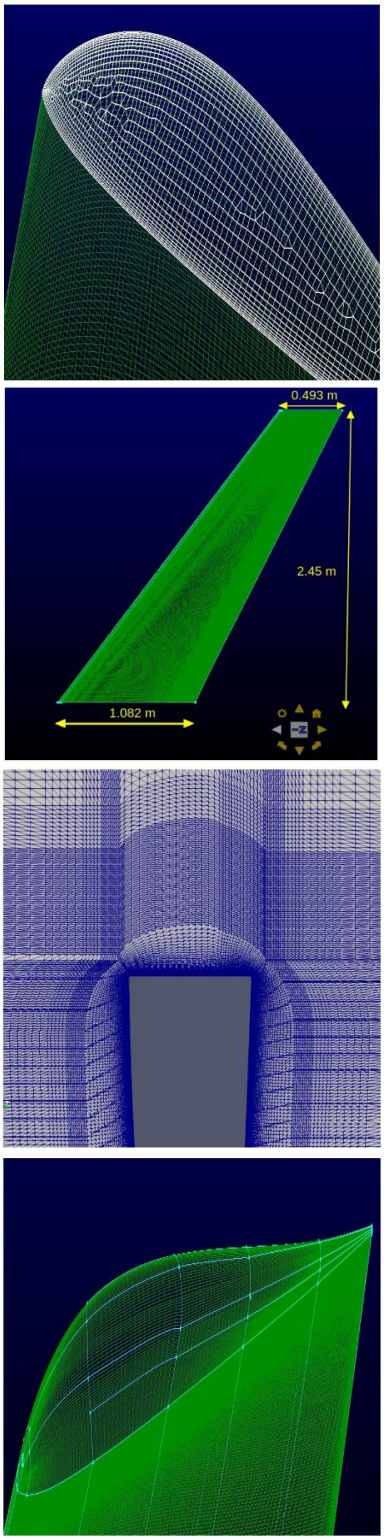


**Fig. 1:** From left to right: A surface mesh of the Flat Wing Tip FWT (left), the Rounded Wing Tip RWT, an axial cross-section of the volume FWT mesh, and the wing planform

**DOI: 10.3844/jastsp.2025.1.11**

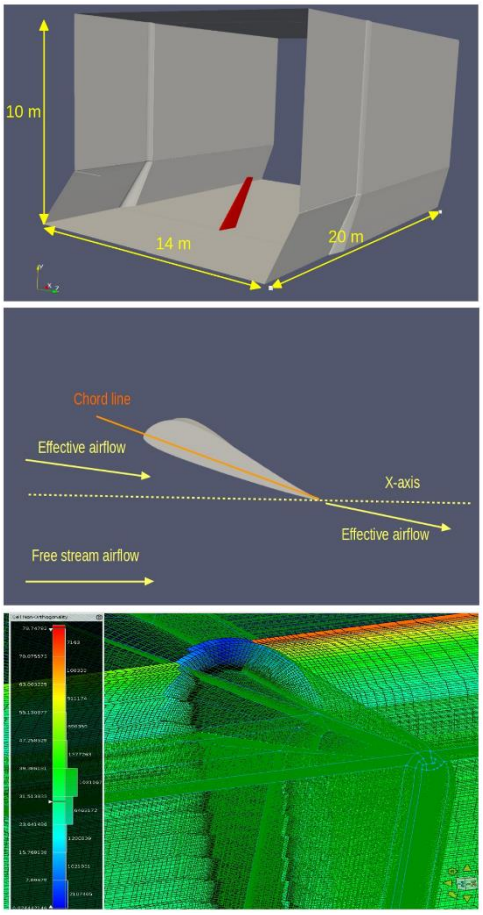


**Fig. 2:** Dimensions of the computational mesh (left), Inflation layers formed around the rounded wing tip (middle), kinematics of the flow around the airfoil (right)

## Results and Discussion

The wing geometry is tabulated in Table (1) and illustrated in Fig. (1). This is about a swept back wing of relatively low Aspect Ratio (AR) which is twisted about 5 degrees so that the lift distribution and tip stall characteristics are optimized. Such a configuration (low AR, sweeping) is expected to produce high induced drag, especially at low speeds and Angle Of Attack (AOA). To this end, a comprehensive aerodynamic performance estimation is attempted herein aiming at the analysis of flow under two flight conditions, namely level flight at cruise speed and maneuvering at high AOA, while stress is given to the effect of the wing tip geometry on the formation of the vortex. The numerical results are depicted in the form of Pressure Coefficient $C_p$ distributions at several spanwise locations of the wing as well as the produced total lift and drag. The flow is illustrated by field distributions on cross-flow planes at axial positions in the wake and the wing tip vortex depiction along with the streamlines. The wake formation and strength are also estimated through flow field distributions in directions crossing the wake at several axial positions. The effective angle of attack as well as the angle of induced downwash are estimated spanwise while the strength of spanwise flow is estimated through the diversion of streamlines. The mean fields were obtained by averaging over a period of 1 sec which corresponds to around 40 non-dimensional time units (one time unit is the time it takes for the flow to run 1 mean chord of the wing). This time window is estimated as adequate for obtaining statistically stationary results since the main aerodynamic performance metrics (lift and drag) are stabilized.

### *Cruise Condition ($AoA = 5^o, V_{cruise} = 36.52$ m/s)*

The flow under cruise conditions is depicted in Fig. (3). It is readily concluded that the flow is more attached to the rounded wing tip whereas the flow detaches from the flat wing tip and gives rise to a strong wing tip vortex downstream. The strength of the vortex is measured by the downwash (velocity magnitude in the negative lift direction) which reaches the values $U_z\,min = 7 m/s$ by the RWT case whereas the FWT is stronger, namely $U_z\,min = 8\ m/s$. This tip vortex strength variation and the subsequent low-pressure region in the vortex have an effect on the loading of the wing as depicted in Fig. (4). The flow on the pressure side has a constant inclination to the wing tip which is attributed to the leak of flow from the pressure side to the suction side. On the contrary, on the suction side, the flow initially deviates towards the tip but immediately diverts to the root as being driven by the wing tip leak flow. Due to the stronger vortex by the FWT case, this diversion is more prominent than the RWT geometry thus leading to a reduction of the axial component of the velocity, $U_x\,max = 49\ m/s$ vs. $U_x\,max = 52\ m/s$ and subsequently to a reduction of pressure suction and $Cp$ distribution (Fig. 5) which is extended at least up to the half span of the wing.

### *Maneuvering Condition ($AoA = 14^o, V_{cruise} = 36.52$ m/s)*

The analysis of the flow under maneuvering conditions is attempted through a detailed examination of the turbulence character in the near wing tip wake for both FWT and RWT cases. The streamwise locations of the plane cut as well as the quantities to be examined are tabulated in Table (2).

**Table 1:** Geometry of the wing

| | |
|---|---|
| Tip Chord [m] | 0.493 |
| Root Chord [m] | 1.082 |
| Semi Span [m] | 2.45 |
| Twist [deg] | 4.9 |
| Sweep ($\Lambda_{c/4}$) [deg] | 33 |
| Mean Chord [deg] | 5.94 |
| Aspect Ratio (AR) | 5.94 |
| Taper Ratio | 0.45 |

**DOI: 10.3844/jastsp.2025.1.11**

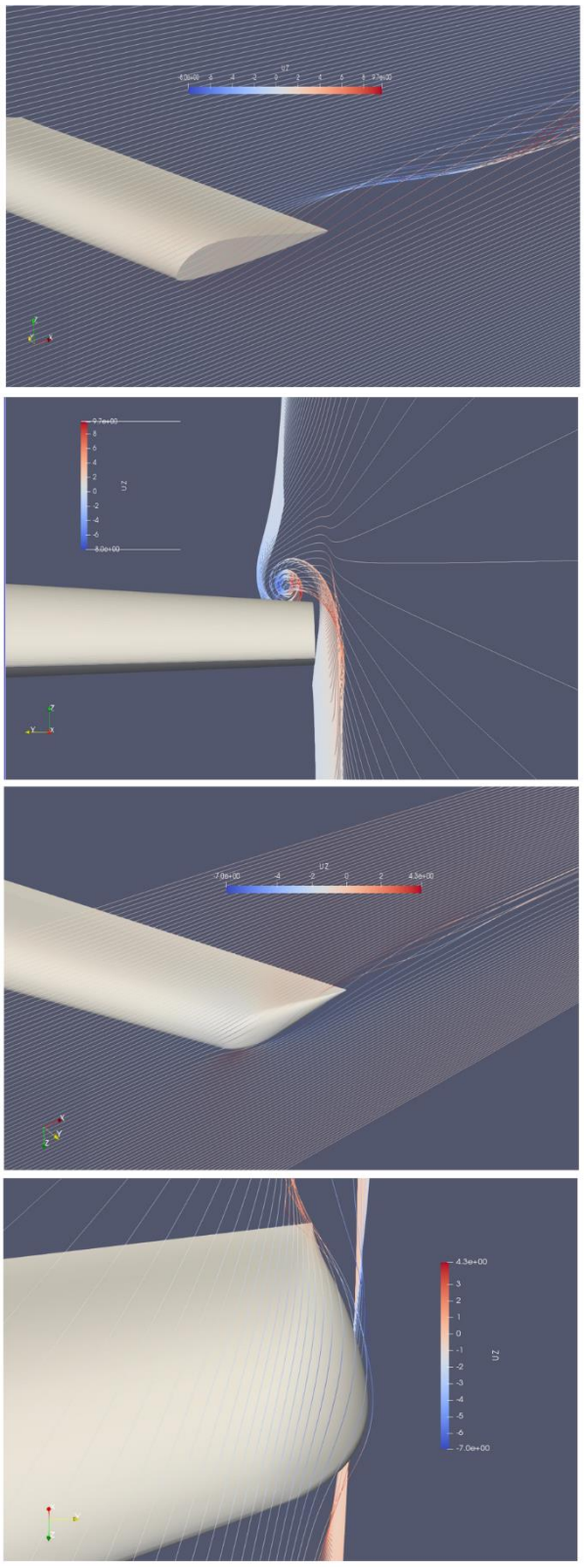

**Fig. 3:** Streamlines around FWT and RWT wing (lateral and front views). The magnitude of the Z component of velocity (Lift direction) is depicted on the streamlines

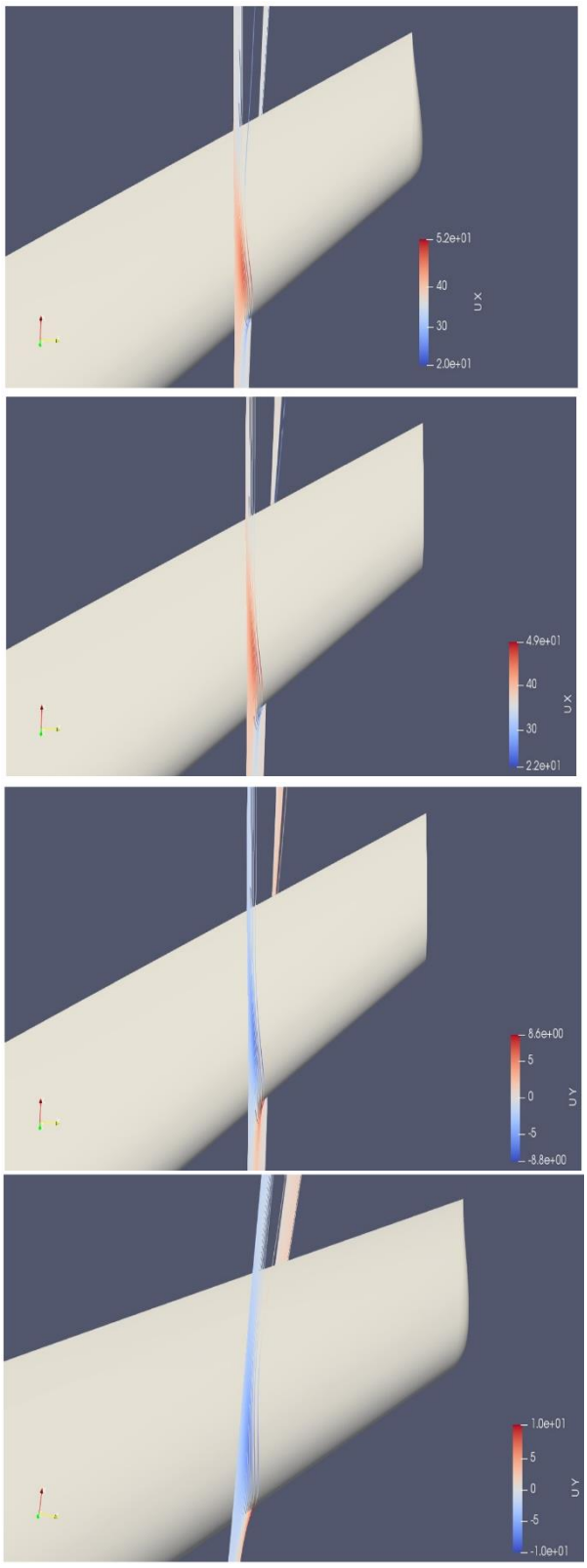

**Fig. 4:** Streamlines of the flow as approaching the wing along (flat vs. rounded wing tip) with contours of velocity components

**DOI: 10.3844/jastsp.2025.1.11**

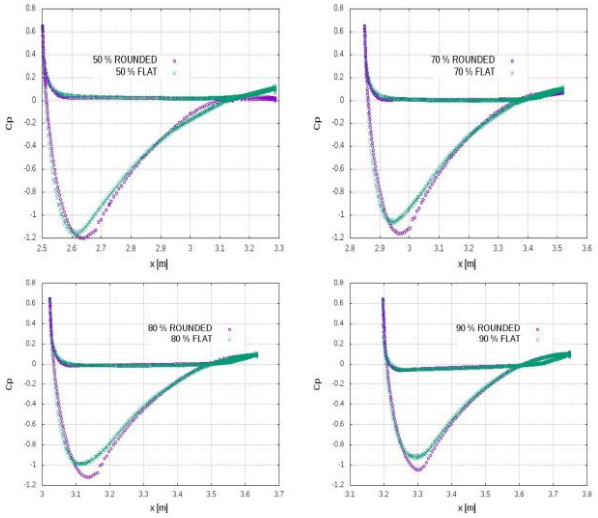


**Fig. 5:** $C_p$ distribution at several spanwise locations of the wing at level flight

**Table 2:** Aerodynamic performance of wing with two tip configurations at several flight conditions

| Abbreviation | Description |
|---|---|
| XC0 | Cross section at 20% of tip chord measured from the leading edge |
| XC01 | Cross section at 40% |
| XC1 | Cross section at 80% |
| XC2 | Cross-section plane at 99% |
| XC3 | Cross-section plane at 110% |
| XC4 | Cross section at 150% |
| XC5 | Cross section at 200% |
| P | Instantaneous static pressure (P = 0 atmospheric datum pressure) |
| U | Instantaneous Axial Velocity |
| $= \frac{^{norm}_{x}C_{tip}}{U_{inf}}$ | Instantaneous normalized axial vorticity |
| UPrime2Mean | The prime-squared mean of the velocity field |

## *Characteristics of Turbulence*

The axial velocity distribution at several cross-sections downstream is depicted in Fig. (6) for the FWT case. A considerable surplus of axial velocity is identified in the vortex core which is caused by a pressure drop. The measured axial velocity reaches the maximum value of 1.5 $U_{\text{inf}}$ at XC3 which is diminished to 1.12 $U_{\text{inf}}$ at XC5, Fig. (7), middle, while the static pressure deficit also diminishes downstream. The width of the vortex increases downstream in the pressure side (the freestream axial velocity is reached in higher $z$ values downstream) while at the same time, the vortex loses in strength downstream as the normal axial vorticity diminishes. The downstream meandering of the wake to the suction side (decreasing z) from XC3-XC4 and subsequently to the pressure side (XC4-XC5) is also obvious as being identified by the location of minimum Pressure (P) which defines the center of the vortex. The contours of the quasi-spanwise spanwise velocity component are shown in Fig. (8) where an early formation (at XC0) of the spanwise flow (outboard at the pressure side and inboard at the suction side) is established. This gives rise to a high-speed cross-flow velocity, Fig. (10) which increases chordwise. The boundary layer does not have the energy to stay on the flat wing tip contour and detaches at the two corners of the tip, thus forming the shear layers which are regions of high shear stress that are recognized by high values of the Prime Squared Mean of the Axial Velocity (PSMAV), Fig. (9).

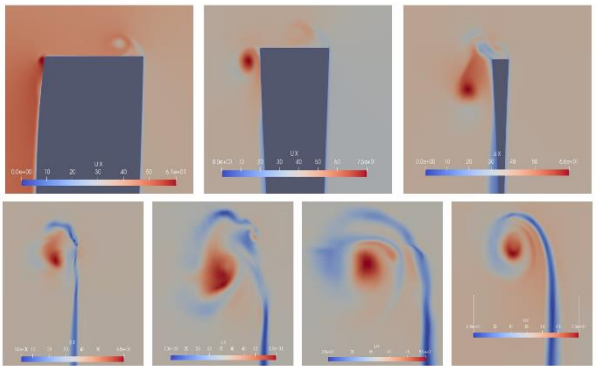

**Fig. 6:** Contours of axial velocity component from XC0 to XC5 (from left to right)

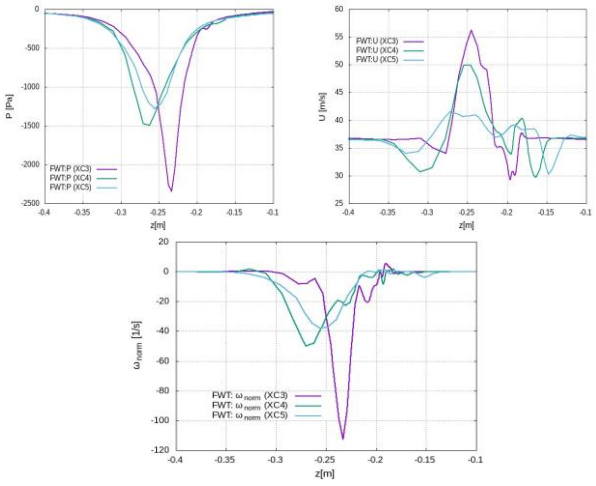


**Fig. 7:** FWT: Distribution of P, U, $\omega_{norm}$ across a line at a spanwise plane passing through the vortex core center

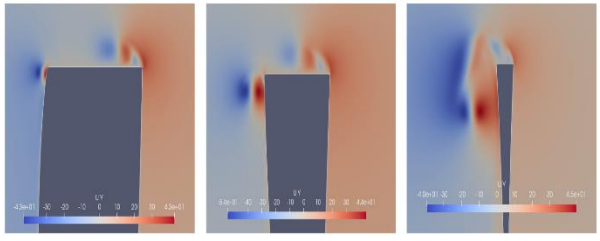

**DOI: 10.3844/jastsp.2025.1.11**

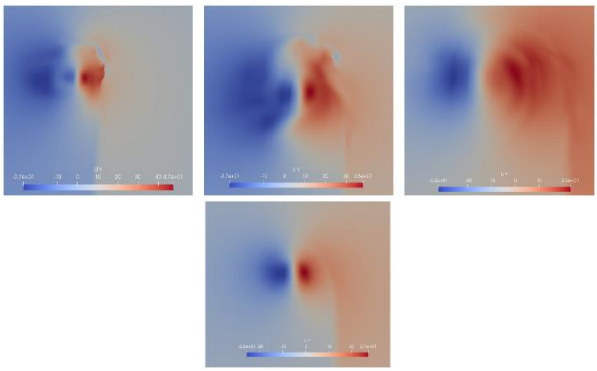

**Fig. 8:** FWT: Contours of velocity y-component from XC0-XC5 (from left to right)

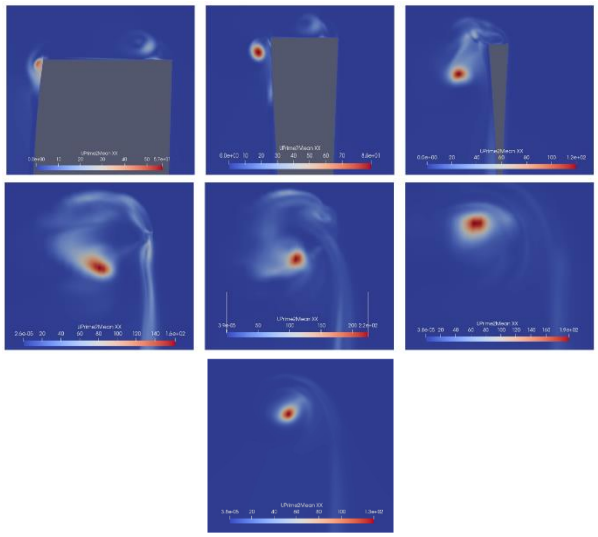

**Fig. 9:** FWT: Contours of Reynolds stress $u^0$ $u^0$ from XC0-XC5 (left to right).

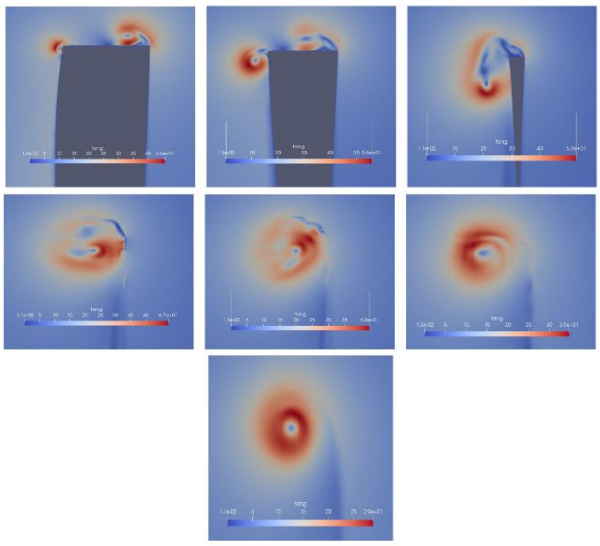

**Fig. 10:** FWT: Contours of cross-flow velocity magnitude from XC0-XC5 (left to right)

The process of vortex formation is identified as the emergence of two shear layers at the tip corners (the suction side one is stronger/high PSMAV), Fig. (9), which circumvent the tip and merge. The PSMAV increases by moving to the trailing edge reaching the maximum value of Root-Mean-Squared (RMS) of PSMAV 0.42 $U_{inf}$ at XC3. The high-level turbulence regions (shear layers) are wrapped up, then they are mixed and gradually form a coherent vortex which is recognized in Fig. (10) where the minimum cross-flow velocity (0.01 m/s) depicts the center of the vortex. Finally, the four-leaf clove pattern of the Reynolds shear stress bar (v'w') is observed in Fig. (11) where the Reynolds stress is shifted 45 deg from the corresponding mean strain rate, Fig. (12) which is also verified experimentally by Chow *et al*. (1997) and numerically in a Large Eddy Simulation being conducted by Jiang *et al*. (2008). This fact hints that the Boussinesq eddy viscosity assumption which is the basis of the isotropic linear eddy viscosity model does not hold in the high anisotropic field of the wing tip vortex.

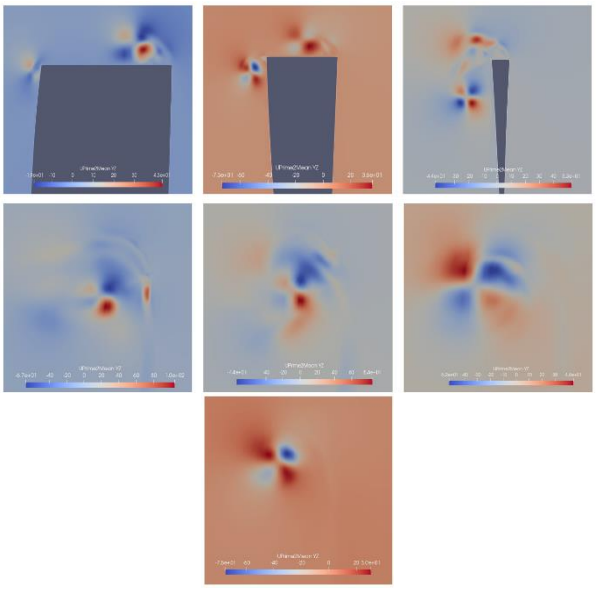

**Fig. 11:** FWT: Contours of Reynolds stress $v^0$ $w^0$ from XC0-XC5 (left to right)

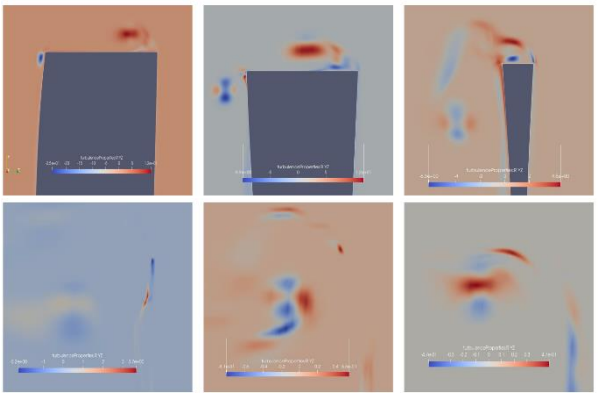

**DOI: 10.3844/jastsp.2025.1.11**

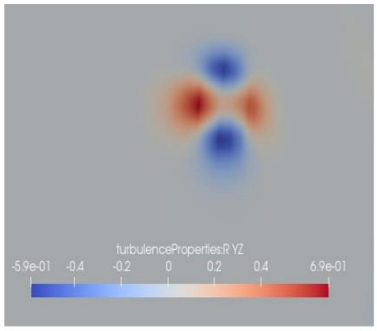


**Fig. 12:** FWT: Contours of the mean strain rate $-\left(\frac{\partial v}{\partial z}+\frac{\partial w}{\partial y}\right)$ from XC0-XC5 (left to right)

The wake formation by the RWT case follows a different pattern. The boundary layer has enough energy to circumvent the round wingtip due to smooth change in curvature up to XC01 (no obvious change of axial velocity, Fig. 13). At XC1 a high turbulence region is identified (RMS of PSMAV equal to 2.08 $U_{\text{inf}}$ and high axial velocity equal to 2.32 $U_{\text{inf}}$, see also Fig. 14), which rotates and mixes strongly with the wake of the wing at XC2. This results in a rapid deceleration of a vortex whose core exhibits an axial velocity deficit of 0.54 $U_{\text{inf}}$ at XC4 and 0.3 $U_{\text{inf}}$ at XC5. The static pressure distribution from XC4-XC5, Figs. (15-16), verifies the higher pressure drop at axial cross sections by the FWT case in comparison to RWT which means higher axial velocities. The mixing of wake and tip vortex at the trailing edge region which decelerates the vortex by the RWT case is illustrated in Fig. (17), right. In the same picture, left, the vortex is depicted to accelerate while the velocity in the wake region is much smoother by the FWT case. In terms of the wing loading, this is examined through the streamlines of the flow, Fig. (18) which emanate from the 95% of span positions. It is readily concluded that by RWT the high velocity/high turbulence roll-up of the flow which is identified at XC1 (80% of the chord) as axial velocity excess and in Fig. (19), right as pressure drop on the suction side near the tip conduces to the direction of the flow more inboard on the suction side and more outboard on the pressure side in comparison to FWT. This conduces to higher loading of the wing since the velocity component normal to the quarter chord line, which is correlated to aerodynamic loading, increases by such flow diversion. The effect of the wing tip vortex on wing pressure distribution persists at least up to 50% of the wing span as depicted by the $C_p$ distribution at several spanwise locations in Fig. (20). Grid-independent results, in terms of wing loading, are also verified by the coincidence of $C_p$ distributions of the FLAT and FLAT COARSE (coarser mesh) cases.

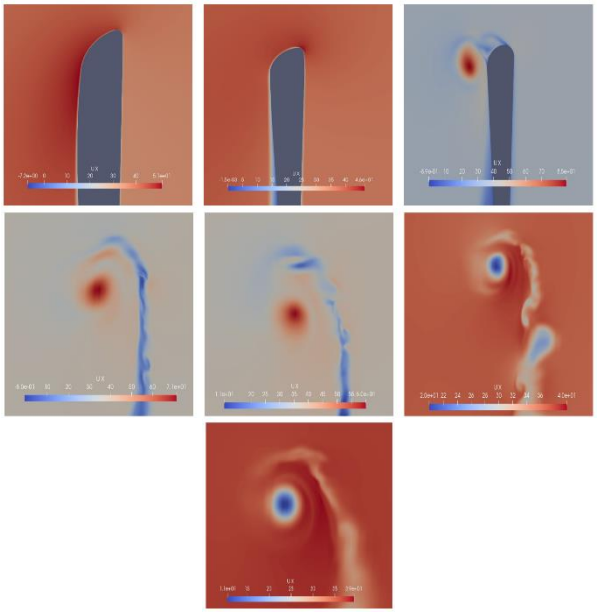

**Fig. 13:** RWT: Contours of axial velocity component from XC0-XC5 (from left to right)

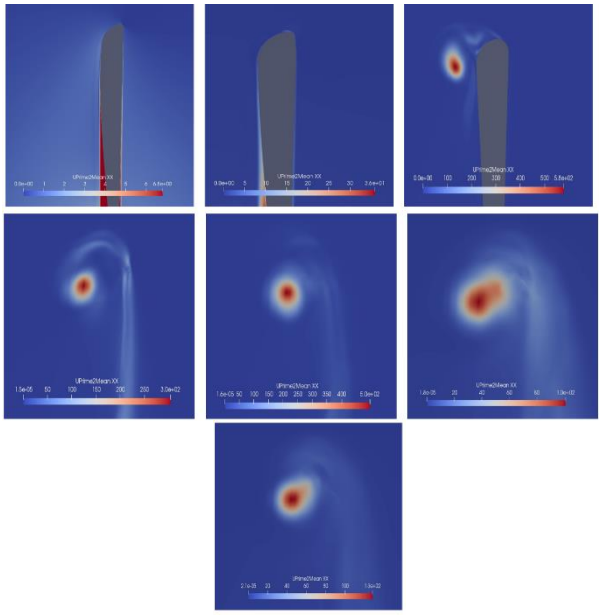

**Fig. 14:** RWT: Contours of Reynolds $u^0$ $u^0$ stress from XC0-XC5 (left to right)

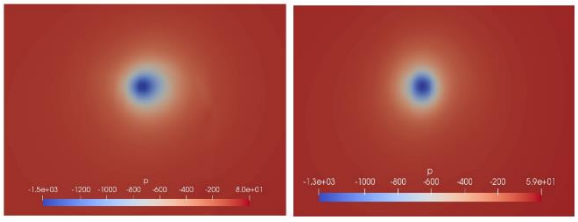

**DOI: 10.3844/jastsp.2025.1.11**

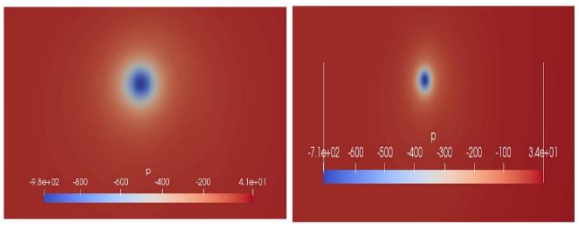

**Fig. 15:** FWT: P contours in the wake (XC4-XC7, from left to right)

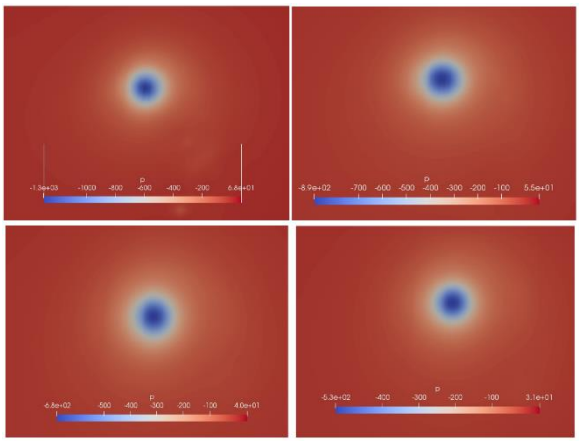

**Fig. 16:** RWT: P contours in the wake (XC4 to XC7, from left to right)

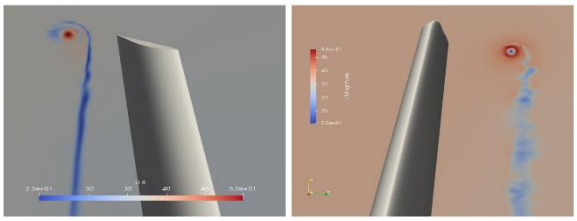

**Fig. 17:** Details of the velocity field at XC4 (FW left, RWT right)

The wing approaching and leaving flow is also examined in terms of the effective angle of attack $\alpha_{eff}$ and the angle of induced downwash $\epsilon$. The former is the angle between the incoming velocity vector and the chord line while the latter is the angle of the outgoing velocity vector and the horizontal axis. The free stream airflow is assumed to be aligned with the x-axis, Fig. (2), right. The sampling points at spanwise locations are along the chord line ranging up to approximately 0.35 m from the leading and trailing edge. The results are depicted in Fig. (21) from where it is deduced that the effect of the wing tip vortex on the $\alpha_{eff}$ is considerable in both FWT and RWT cases. A reduction of more than five degrees in $\alpha_{eff}$ is identified between the airfoils at 50 and 90% in both configurations which results in subsequent lift reduction.

In terms of $\epsilon$ by FWT this is relatively constant along the examined spanwise positions which hints at the favorable elliptical lift distribution, as stated by Anderson (2016). On the contrary by RWT, the values of spanwise are highly fluctuating which is attributed to the high mixing of the tip vortex and wing wake.

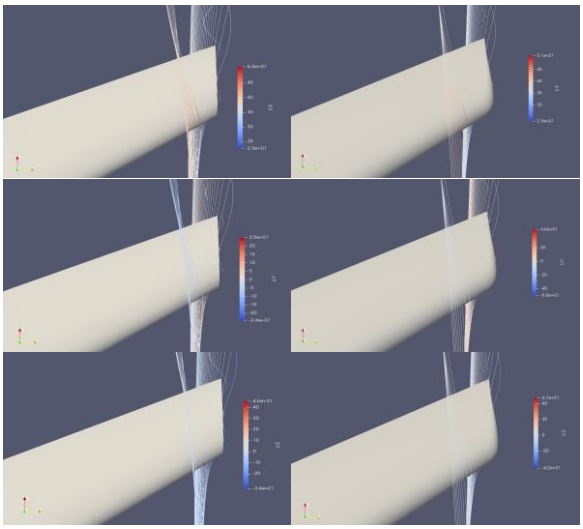

**Fig. 18:** Streamlines of the flow along 95% of the span along with the contours of velocity components. FWT (left column) vs. RWT (right column)

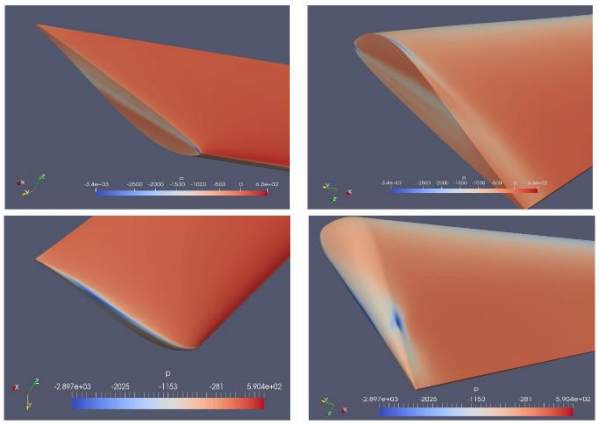

**Fig. 19:** Pressure distribution on pressure and suction side for FWT and RWT configuration

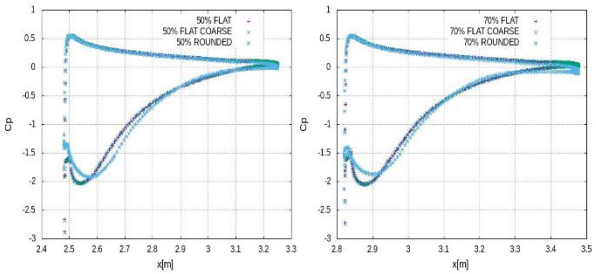

**DOI: 10.3844/jastsp.2025.1.11**

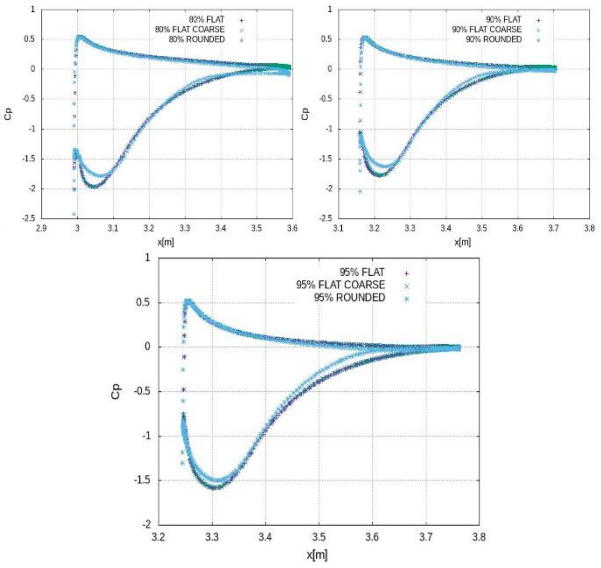


**Fig. 20:** $C_p$ distribution at several spanwise locations of the wing under maneuvering conditions

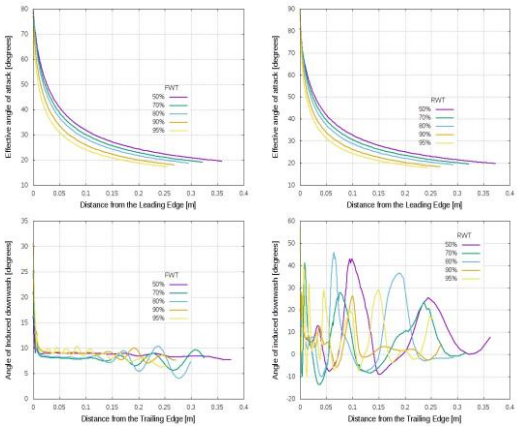


**Fig. 21:** Effective angle of attack (FWT and RWT) and angle of induced downwash (FWT and RWT) from left to right

**Table 3:** Aerodynamic performance of wing with two tip configurations at several flight conditions

| Conditions | Wing Tip Geometry | Pressure Drag [Nt] | Viscous Drag [Nt] | Total Drag [Nt] | Lift [Nt] | Lift to Drag Ratio (L/D) | Gain (%) in L/D |
|---|---|---|---|---|---|---|---|
| Cruise Conditions | FLAT | 22.99 | 14.25 | 37.24 | 667.35 | 17.92 | - |
| Cruise Conditions | Rounded | 21.85 | 11.41 | 33.26 | 665 | 19.99 | 11.5 |
| Maneuvering Conditions | Flat | 123.77 | 11.99 | 135.76 | 1555.68 | 11.46 | - |
| Maneuvering Conditions | Rounded | 111.47 | 12.13 | 123.6 | 1610 | 13.02 | 13.6 |

Finally, in terms of metrics of aerodynamic performance (Life and Drag), the results of cruise and maneuvering flight conditions for both FWT and RWT configurations are tabulated in Table (3). In both cases, the lift to drag ratio by RWT configuration is higher than the FWT one. At cruise conditions where the pressure and drag are relatively small, the gain is in terms of viscous drag reduction while the lift change is negligible. At maneuvering conditions, the viscous drag by RWT is marginally higher than FWT which may be attributed to the strong roll-up of the wake. The pressure drag by RWT is considerably lower than FWT since the vortex has less kinetic energy while the lift by RWT is also higher than FWT due to the strong inboard diversion of the flow which is favorable by swept-back wings.

## Conclusion

The current study focuses on the formation of the wing tip vortex around a low-speed aircraft's swept back wing of a relatively low aspect ratio. Two configurations of the wing tip and two flight conditions were examined aiming at the quantification of the effect of the tip vortex on the aerodynamics of the wing. Apart from the metrics such as lift and drag a thorough investigation of the turbulence was attempted. The main findings of the flow read as follows:

- The swept-back wings exhibit a considerable spanwise flow which increases steeply with the angle of attack as depicted by the streamlines at the outboard of the wing
- The mechanism of wing tip vortex formation differentiates by rounding the wing tip at high angles of attack. By the flat wing tip, the boundary layer initially detaches at the two tip corners thus two shear layers are formed which subsequently roll up and merge to form a coherent vortex. In contrast, by the rounded wing tip, a compact vortical structure of high velocity and turbulence detaches and merges with the wing wake. These two mechanisms lead to a tip vortex with a significant axial velocity surplus by FWT and a strong deficit by RWT
- By all flight conditions, the effect of tip vortex on wing loading extends at least to the half of wing's semi-span as depicted by the $C_p$ distributions. By the high angle of attack condition, the effective angle of attack can reduce up to 5 degrees from the half of the span to the tip thus compromising lift production. In the RWT case, a strong mixing of wake and tip vortex causes a high fluctuating, non-uniform distribution of the angle of induced downwash which hints at discrepancies with the favorable elliptical lift distribution of the wing, in contrast with the FWT case
- Rounding the wing tip leads to an increased lift-to-drag ratio at both flight conditions. Nevertheless, by high angles of attack, the RWT produces a more fluctuating wake, at least in the near field, which may have an effect on the stability of the aircraft if the trailing flow affects the empennage

The numerical method verifies that some shear Reynolds stresses are shifted 45 deg from the corresponding mean strain rate in the rolling wing tip vortex which is also verified numerically and experimentally. This fact shows the deficiency of linear eddy viscosity turbulence models to predict accurately such flows. Special attention is advisable if the wing wake interacts with other parts of the aircraft.

## Acknowledgment

This study was supported by computational time granted from the National Infrastructures for Research and Technology S.A. (GRNET S.A.) in the National HPC facility - ARIS - under project ID 1111".

## Funding Information

The two authors of this manuscript did not receive any fund for the implementation of the relative research and the writing of the text.

## Author's Contributions

**Nikolaos Konstantinos Lampropoulos:** Conceptualized and materialized the high-fidelity numerical simulation of wing tip vortex flow.

**Ioannis Eleftherios Sarris:** Participated in writing and editing of the text.

## Ethics

To the best knowledge of both authors, no ethical issues may arise after the publication of this manuscript.

## References

Anderson, J. D. (2016). *Fundamentals of Aerodynamics*.

Antoniou, S., Kapsalis, S., Panagiotou, P., & Yakinthos, K. (2023). Parametric Investigation of Leading-Edge Slats on a Blended-Wing-Body UAV Using the Taguchi Method. *Aerospace*, *10*(8), 720. https://doi.org/10.3390/aerospace10080720

Chow, J. S., Zilliac, G. G., & Bradshaw, P. (1997). Mean and Turbulence Measurements in the Near Field of a Wingtip Vortex. *AIAA Journal*, *35*(10), 1561–1567. https://doi.org/10.2514/2.1

Feder, D.-F., Dhone, M., Kornev, N., & Abdel-Maksoud, M. (2018). Comparison of different approaches tracking a wing-tip vortex. *Ocean Engineering*, *147*, 659–675. https://doi.org/10.1016/j.oceaneng.2017.09.036

Jiang, L., Cai, J., & Liu, C. (2008). Large-eddy simulation of wing tip vortex in the near field. *International Journal of Computational Fluid Dynamics*, *22*(5), 289–330. https://doi.org/10.1080/10618560801938883

Liang, Z., & Xue, L. (2014). Detached-eddy simulation of wing-tip vortex in the near field of NACA 0015 airfoil. *Journal of Hydrodynamics*, *26*(2), 199–206. https://doi.org/10.1016/s1001-6058(14)60022-6

O'Regan, M. S., Griffin, P. C., & Young, T. M. (2016). A vorticity confinement model applied to URANS and LES simulations of a wing-tip vortex in the near-field. *International Journal of Heat and Fluid Flow*, *61*, 355–365. https://doi.org/10.1016/j.ijheatfluidflow.2016.05.014

Philippe, R, S. (1997). Comments on the Feasibility of LES for Wings and on the Hybrid RANS/LES Approach. *Proceedings of the First AFOSR International Conference on DNS/LES*, 137–147.

Rajendran, S. (2012). *Design of Parametric Winglets and Wing tip devices : A Conceptual Design Approach*.

Shur, M. L., Spalart, P. R., Strelets, M. Kh., & Travin, A. K. (2008). A hybrid RANS-LES approach with delayed-DES and wall-modelled LES capabilities. *International Journal of Heat and Fluid Flow*, *29*(6), 1638–1649. https://doi.org/10.1016/j.ijheatfluidflow.2008.07.001

Soltani, M. R., Masdari, M., & Tirandaz, M. R. (2017). Effect of an end plate on surface pressure distributions of two swept wings. *Chinese Journal of Aeronautics*, *30*(5), 1631–1643. https://doi.org/10.1016/j.cja.2017.07.008

Spalart, P. R., Deck, S., Shur, M. L., Squires, K. D., Strelets, M. Kh., & Travin, A. (2006). A New Version of Detached-eddy Simulation, Resistant to Ambiguous Grid Densities. *Theoretical and Computational Fluid Dynamics*, *20*(3), 181–195. https://doi.org/10.1007/s00162-006-0015-0